Facile Synthesis of FeCoNiCuIr High Entropy Alloy Nanoparticles for Efficient Oxygen Evolution Electrocatalysis

Chen Cai [1],*, Zongwei Xin [1], Xuefan Zhang [1], Jian Cui [1], Hui Lv [1], Wanjie Ren [1], Cunyuan Gao [2] and Bin Cai [2],*

[1] Shandong Institute of Non-Metallic Materials, Jinan 250031, China
[2] School of Chemistry and Chemical Engineering, Shandong University, Jinan 250100, China
*   Correspondence: caichenyihao@163.com (C.C.); bin.cai@sdu.edu.cn (B.C.)

Abstract: The lack of an efficient and stable electrocatalyst for oxygen evolution reaction (OER) greatly hinders the development of various electrochemical energy conversion and storage techniques. In this study, we report a facile synthesis of FeCoNiCuIr high-entropy alloy nanoparticles (HEA NPs) by a one-step heat-up method. The involvement of glucose made the NPs grow uniformly and increased the valence of Ir. The resulting FeCoNiCuIr NPs exhibit excellent OER performance in alkaline solution, with a low overpotential of 360 mV to achieve a current density of 10 mA cm^{-2} at a Tafel slope of as low as 70.1 mV dec^{-1}. In addition, high stability has also been observed, which remained at 94.2% of the current density after 10 h constant electrolysis, with a constant current of 10 mA cm^{-2}. The high electrocatalytic activity and stability are ascribed to the cocktail effect and synergistic effect between the constituent elements. Our work holds the potential to be extended to the design and synthesis of high-performance electrocatalysts.

Keywords: high entropy alloy; oxygen evolution reaction; electrocatalyst; nanoparticle

1. Introduction

The development of highly efficient water-splitting electrocatalysts is essential for addressing the worsening energy crisis and long-term environmental pollution [1–5]. However, the large-scale application of water-splitting devices is limited by the slow kinetics of the oxygen evolution reaction (OER) at the anode [6–11]. Currently, Ir-based materials represent the most active electrocatalyst candidate for catalyzing OER [12–18]. Unfortunately, Ir is a very rare element with an abundance about 10 times lower than that of Pt, resulting in the high cost of Ir-based electrocatalysts [14]. Therefore, how to reduce the usage of noble Ir, while maintaining the high catalytic activity, becomes the main focus of researchers. An effective strategy to both reduce the usage of noble metals and improve the catalytic activity is to make multimetallic alloys with transition metals, owing to the synergistic effects between various components. The alloyment with distinct elements can facilitate the adsorption/desorption of various reaction intermediates or regulate charge transfer, thus promoting the overall reaction rate. In addition, structural optimization of multimetallic alloys is crucial for maximizing the exposure of active sites and improving long-term stability. Although tremendous efforts have been devoted in this direction, there remains a large room for further tuning the electronic structure of alloyed catalysts and improving the catalytic efficiency.

High-entropy alloys (HEAs), defined as single-phase alloys containing five or more elements, have attracted extensive attention in the electrocatalysis community, owing to the unusual physicochemical and mechanical properties [19–22]. The synergistic effect of alloy elements led to HEAs with stable and tunable electronic structures, which demonstrated notable, metal-like catalytic activities and enhanced durability [23]. The catalytic interfaces of HEAs consist of numerous atomic coordination environments as active sites, where the local structural and electronic properties could be optimized to overcome the limitations

of conventional catalysts [24,25]. Tuning the binding energy of reaction intermediates has been regarded as an essential way to optimize the catalytic performance [19,26]. Therefore, it is reasonable to deduce that Ir-based HEAs hold the potential to tune the electronic structure of Ir sites by combining with cheap transition metals, which remain in their infancy stage [27]. In addition, control of size of HEA nanostructures is believed to improve catalytic performance. However, reliable and scalable synthesis strategy of nanosized HEAs remains a challenging task.

In this work, we describe a facile synthesis for FeCoNiCuIr HEA nanoparticles (NPs) with a tunable size ranging from 16 to 32 nm. The resulting FeCoNiCuIr NPs exhibit excellent OER performance in alkaline solution, with a low overpotential of 360 mV to achieve a current density of 10 mA cm^{-2} at a Tafel slope of as low as 70.1 mV dec^{-1}. After 10 h of constant electrolysis at a constant current of 10 mA cm^{-2}, the as-obtained HEA NPs maintained 94.2% of the initial current density, indicative of a high durability. The high electrocatalytic activity and stability are ascribed to the cocktail effect and synergistic effect between the constituent elements. This synthesis strategy holds the potential to be extended to other HEAs with different compositions.

2. Results and Discussion

The FeCoNiCuIr HEA NPs were synthesized through a simple one-pot oil phase heat-up method at 220 °C. Figure 1a,b show the transmission electron microscopy (TEM) images of FeCoNiCuIr HEA NPs synthesized with and without the presence of glucose, which display irregular morphologies for both types of HEA NPs. As indicated in the particle size distribution shown in the insets, the presence of glucose increases the average diameter of the HEA NPs to ~32 nm with relatively narrow size distribution, while HEA NPs synthesized without glucose exhibit a smaller diameter (~16 nm) with a larger size distribution. Figure 1c shows the X-ray diffraction (XRD) pattern of the FeCoNiCuIr HEA NP, both of which exhibit a face-centered cubic (FCC) structure. The two diffraction peaks at 43.3° and 50.4° could be ascribed to the (111) and (200) planes. Compared to the diffraction pattern of iridium, the position of the diffraction peaks is obviously shifted, indicating that the lattice parameters of the HEA NPs are smaller than those of the iridium unit cell.

As shown in Figure 1d,e, the high-resolution TEM and corresponding fast Fourier transform (FFT) filtered TEM images show a lattice spacing of 0.21 nm of the as-synthesized FeCoNiCuIr HEA NPs (Figure S1), which is inconsistent with the XRD analysis. The alloy effect was also evaluated by the elemental maps (Figure 1f), which demonstrate a homogenous distribution of all elements within a single particle. X-ray photoelectron spectroscopy was further performed to investigate the electronic structure of Ir sites (Figure S2), which shows a shift of the binding energy of Ir 4f peaks to higher energies upon the addition of glucose to the synthesis system. The percentage of Ir^{4+} in FeCoNiCuIr HEAs with glucose increased, compared to FeCoNiCuIr HEAs without glucose (Table S1). It indicated that the valence state of Ir is increased for the glucose-assisted HEA NPs, which holds promise for OER electrocatalysis [28–30]. Based on these results, the addition of glucose not only changes the size of the HEA NPs, but also increases the valence state of Ir sites.

In order to evaluate the electrocatalytic performances, the FeCoNiCuIr HEA NPs were dispersed on high-surface-area carbon black and further treated by calcination at 200 °C to remove residual surfactants. The OER activity and stability of the FeCoNiCuIr HEA NPs were investigated by a series of electrochemical tests in alkaline solutions. As shown in Figure 2a, the cyclic voltammetry (CV) curves of the two types of HEA NPs and commercial IrO$_2$ were obtained in N$_2$-saturated 1 M KOH at a scan rate of 5 mV s^{-1}, which revealed a higher current density upon the FeCoNiCuIr HEA NPs synthesized in the presence of glucose. The inset shows the comparison of the overpotentials at 10 mA cm^{-2}. The OER overpotential of the FeCoNiCuIr HEA NPs decreased from 410 mV to 360 mV after the introduction of glucose into the synthesis system.
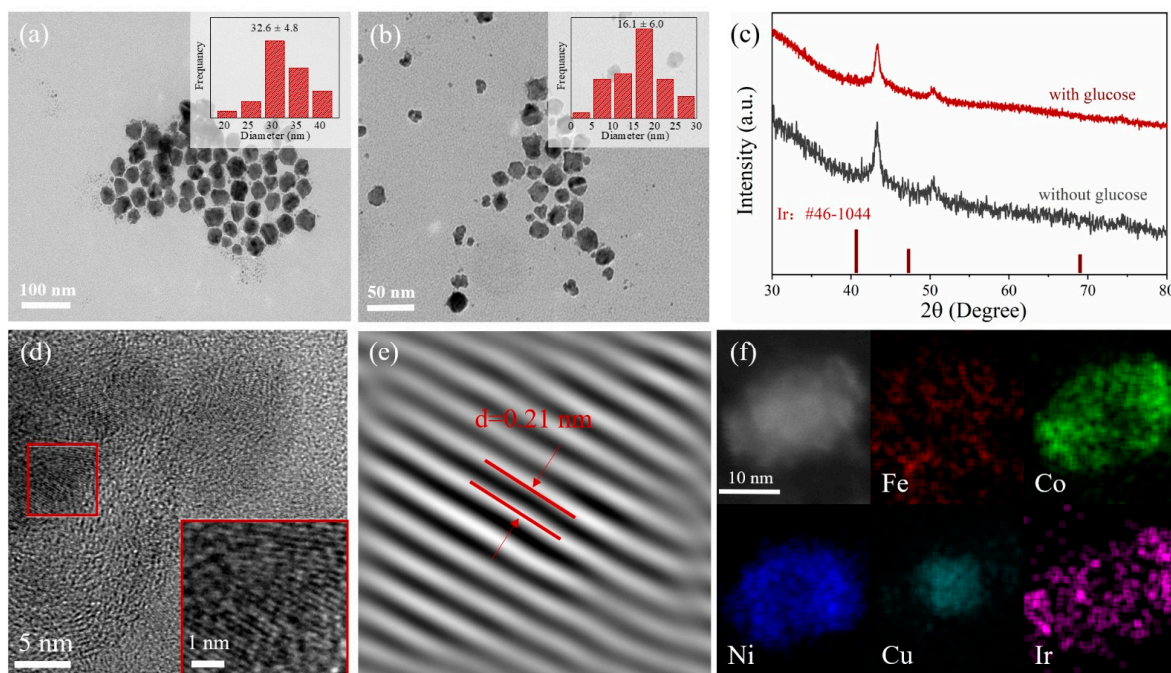
Figure 1. TEM images of FeCoNiCuIr HEA NPs and corresponding particle size distribution (insets) synthesized (**a**) with and (**b**) without the presence of glucose. (**c**) The X-ray diffraction pattern of FeCoNiCuIr HEA NPs. (**d**) HR-TEM, (**e**) corresponding FFT-filtered TEM, and (**f**) elemental maps of FeCoNiCuIr HEA NPs synthesized in the presence of glucose.
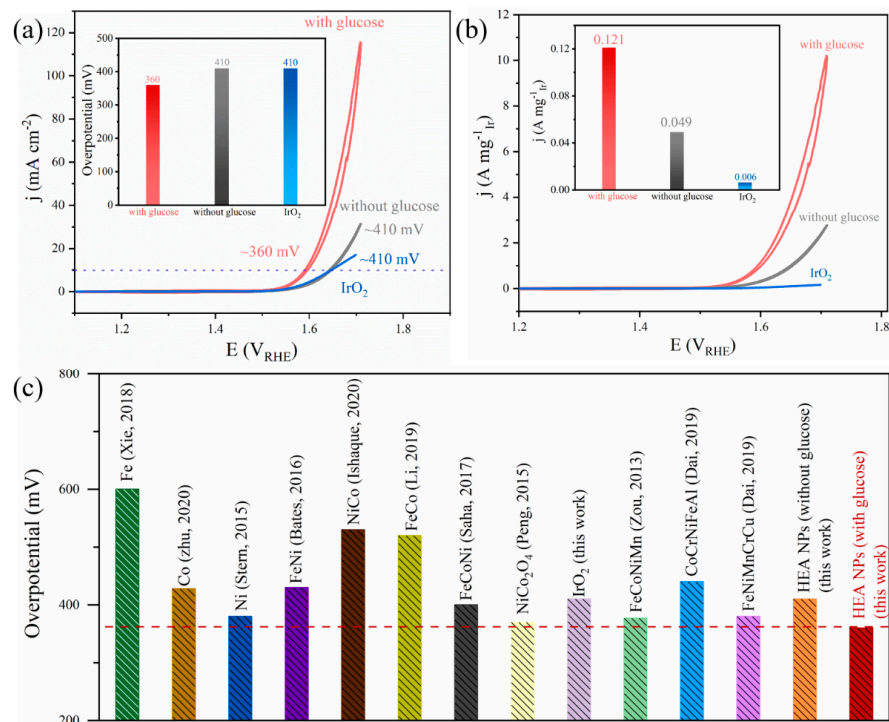

Figure 2. The CV curves of FeCoNiCuIr HEA NPs and commercial IrO_2 normalized by (**a**) electrode surface area and (**b**) Ir mass obtained in N_2-saturated 1 M KOH at a scan rate of 5 mV s^{-1}. Insets display (**a**) the comparison of overpotentials at 10 mA cm^{-2} and (**b**) mass activities at 1.53 V_{RHE} of both types of HEA NPs. (**c**) Comparison of the overpotentials at 10 mA cm^{-2} for metals, bimetallic, trimetallic, commercial IrO_2, and HEA NPs [31–40].

Due to the scarcity of Ir element, the mass activity represents an important parameter for noble-metal-containing electrocatalysts. Figure 2b shows the Ir-mass-normalized CV curves and corresponding mass activities. The optimized FeCoNiCuIr HEA NPs exhibits a mass activity as high as 0.121 A mg^{-1}$_{Ir}$ at 1.53 V$_{RHE}$, while the electrocatalyst synthesized without adding glucose displays a mass activity of 0.049 A mg^{-1}$_{Ir}$, and commercial IrO$_2$ displays a mass activity of 0.006 A mg^{-1}$_{Ir}$. The mass activity of FeCoNiCuIr HEA NPs with adding glucose also outperforms most of the well-developed OER catalysts in literatures (Table S2). As shown in Figure 2c and Table S3, the optimized FeCoNiCuIr HEA NPs even show higher catalytic activity than other previously reported single-element NPs, binary or ternary alloys, commercial IrO$_2$, and other HEAs catalysts [31–40].

Since the CV method often overestimates the OER activity of oxides, herein, we further determined the electrocatalytic activities of the FeCoNiCuIr HEA NPs using steady-state chronopotentiometry at different current densities. As shown in Figure 3a, the potentials required for current densities of 0.1, 0.5, 1, 2.5, 5, and 10 mA cm^{-2} have been plotted, which indicates that the optimized FeCoNiCuIr HEA NPs require less voltages to achieve the same current density. Moreover, the plateaus remain unchanged over time, indicative of a high stability of the HEA NPs. By scrutinizing the Ir-corrected Tafel plots based on steady-state measurements (Figure 3b), we observe that the optimized FeCoNiCuIr HEA NPs give a smaller Tafel slope of 70.1 mV dec^{-1}, in comparison with the HEA NPs synthesized without adding glucose (90.9 mV dec^{-1}).
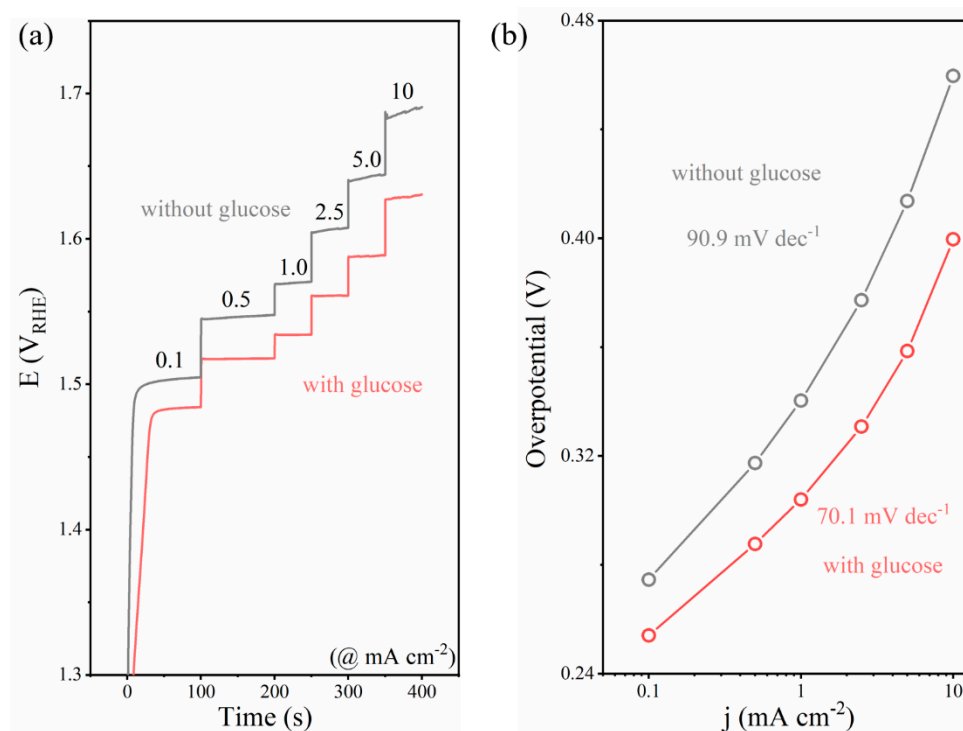

Figure 3. (**a**) The steady-state galvanostatic measurement and (**b**) the corresponding Tafel plots of both types of FeCoNiCuIr HEA NPs, which were obtained at current densities of 0.1, 0.5, 1, 2.5, 5, and 10 mA cm^{-2} in N$_2$-saturated 1 M KOH.

The stability of the as-prepared FeCoNiCuIr HEA NPs was evaluated by both CV cycling for 2000 cycles and chronoamperometry test at 1.59 V$_{RHE}$. As shown in Figure 4a, after 2000 CV cycles, the CV curve displays only slightly decreased current density at high overpotentials, indicative of the excellent stability. The potential for chronoamperometry was set at 1.59 V$_{RHE}$ in order to achieve a current density of 10 mA cm^{-2}. After a 10 h continuous electrolysis, the FeCoNiCuIr HEA NPs maintained 94.2% of its initial current density (Figure 4b). After the durability test, the microstructure and element distribution

of the FeCoNiCuIr HEA NPs were investigated (Figure S3). It is revealed that the five elements are still evenly distributed without obvious element aggregation. These results demonstrate an excellent stability of the FeCoNiCuIr HEA NPs for OER electrocatalysis.
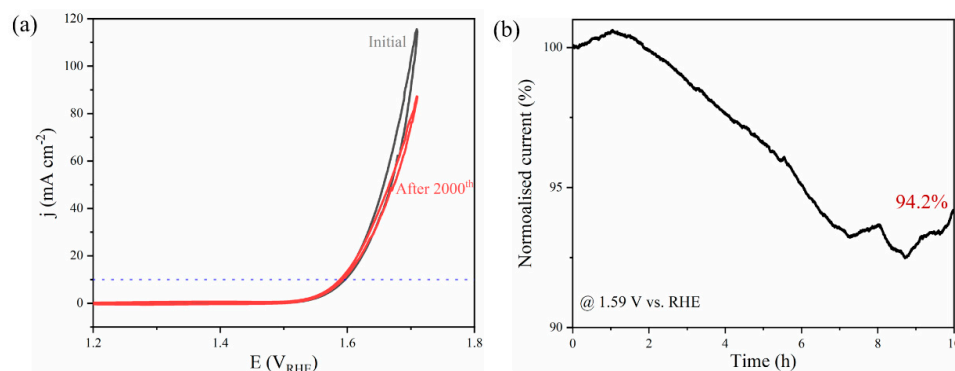

Figure 4. Stability tests for the FeCoNiCuIr HEA NPs using (**a**) CV cycling for 2000 cycles at a scan rate of 50 mV s^{-1} and (**b**) chronoamperometry measurement at 1.59 V$_{RHE}$ in N$_2$-saturated 1 M KOH.

3. Experimental Section

3.1. Chemicals

Iron (III) acetylacetonate, cobalt (III) acetylacetonate, nickel (II) acetylacetonate, copper (II) acetylacetonate, iridium (III) acetylacetonate, molybdenum hexacarbonyl, glucose, oleylamine, ethanol, and n-hexane were purchased from Macklin Biochemical Technology Co., Ltd. (Shanghai, China) Commercial iridium oxide (IrO$_2$) was purchased from Aladdin Chemical. Nafion (5 wt. % in ethanol) solution was purchased from Sigma-Aldrich (Saint Louis, MO, USA). All chemicals were of analytical grade and used as received.

3.2. Synthesis of FeCoNiCuIr HEA NPs

For the preparation of HEA NPs with an average diameter of 32.6 nm, a combination of iron acetylacetonate (8.8 mg), cobalt acetylacetonate (8.9 mg), nickel acetylacetonate (6.4 mg), copper acetylacetonate (6.5 mg), iridium acetylacetonate (12.4 mg), molybdenum hexacarbonyl (33 mg), and glucose (60 mg) are dissolved in oleylamine (5 mL), followed by mixing under sonication. The solution was rapidly heated to 220 °C under the protection of nitrogen atmosphere for 2 h. After cooling down, the solution was then centrifuged to obtain solid precipitate, which was dispersed in hexane. Ethanol was added to wash the products and subjected to centrifugation. At last, the as-obtained HEA nanoparticles were dried in vacuum. The synthesis of HEA NPs with an average diameter of 16.1 nm is similar to the above-described method, except for the absence of glucose.

3.3. Dispersion of FeCoNiCuIr HEA NPs on Carbon Black

A total of 1 mg of HEA and 4 mg of carbon black were dispersed in 10 mL of cyclohexane, followed by sonication to achieve a good mixture. After sonication for 1 h, the product was collected by centrifugation. After drying, the carbon supported FeCoNiCuIr HEA NPs (denoted as FeCoNiCuIr/C) were calcined at 200 °C for 2 h under air atmosphere to remove surface capped ligands [41].

3.4. Electrochemical Measurements

The catalyst ink was prepared by dispersing 1 mg FeCoNiCuIr/C catalysts in a mixture of 495 µL water, 495 µL isopropanol, and 10 µL Nafion solution by sonication for 1 h. Afterwards, FeCoNiCuIr/C catalyst with the concentration of 1 mg mL^{-1} was obtained. Electrochemical measurements were conducted on a CHI 760E Electrochemical Workstation (Chenhua Instrument Corporation, Shanghai, China) in a conventional three-electrode cell. A Pt wire was used as the counter electrode, and a mercuric oxide electrode was used as the reference electrode. The working electrode was a glassy carbon electrode (GCE,

diameter: 3 mm, area: 0.07065 cm^2). Ten microliters of the catalyst ink were dropped onto the GCE surface for further electrochemical tests. All the potentials reported in this work were converted to the reversible hydrogen electrode (RHE). Electrochemical impedance spectroscopy (EIS) measurements were measured in the frequency range from 10 kHz to 0.01 Hz in 1 M KOH solution. The OER performance of the catalysts was evaluated by CV with a scan rate of 5 mV s^{-1} in 1 M KOH solution, and all polarization curves were 95% Ir-corrected. The durability tests were performed in 1 M KOH solution using the chronoamperometric method, and 2000 CVs were also measured to evaluate the stability of catalysts.

3.5. Characterizations

The X-ray diffractometer testing instrument was a SmartLab diffractometer equipped with a copper X-ray source from Rigaku, Tokyo, Japan—with a power of 9 kW, a tube voltage of 45 kV, a tube current of 200 mA, a test range of 20–90°, and a scanning speed of 10°/min. The XPS spectra were collected in a Thermo Fisher ESCALAB Xi+ (Waltham, Massachusetts, USA) with the monochromatic Al Kα X-ray source to analyze the element content and valence. Transmission electron microscopy (TEM) analysis was performed on a Tecnai G2 20 (FEI) at an accelerating voltage of 200 kV. High-resolution TEM was performed on a Titan 80-300 (FEI) microscope operated at an accelerating voltage of 300 kV (Waltham, MA, USA).

4. Conclusions

In conclusion, we developed a facile oil-phase method for the synthesis of FeCoNiCuIr HEA NPs. We found that glucose plays an essential role in the formation of HEA NPs, which could influence the resulting particle size distribution and Ir valence. By adding glucose to the synthesis system, the optimized FeCoNiCuIr HEA NPs exhibit excellent OER performance in 1 M KOH, with a low overpotential of 360 mV to achieve a current density of 10 mA cm^{-2} at a Tafel slope of as low as 70.1 mV dec^{-1}. The as-synthesized FeCoNiCuIr HEA NPs also display excellent stability by maintaining 94.2% of the initial current density after 10 h continuous electrolysis. This facile synthesis strategy is expected to be extended to other HEAs with different compositions.

References

1. Seitz, L.C.; Dickens, C.F.; Nishio, K.; Hikita, Y.; Montoya, J.; Doyle, A.; Kirk, C.; Vojvodic, A.; Hwang, H.Y.; Norskov, J.K.; et al. A highly active and stable $IrO_x/SrIrO_3$ catalyst for the oxygen evolution reaction. *Science* **2016**, *353*, 1011–1014. [CrossRef] [PubMed]

2. Yuan, S.; Peng, J.; Cai, B.; Huang, Z.; Garcia-Esparza, A.T.; Sokaras, D.; Zhang, Y.; Giordano, L.; Akkiraju, K.; Zhu, Y.G.; et al. Tunable metal hydroxide–organic frameworks for catalysing oxygen evolution. *Nat. Mater.* **2022**, *21*, 673–680. [CrossRef] [PubMed]

3. Tahir, M.; Pan, L.; Idrees, F.; Zhang, X.; Wang, L.; Zou, J.-J.; Wang, Z.L. Electrocatalytic oxygen evolution reaction for energy conversion and storage: A comprehensive review. *Nano Energy* **2017**, *37*, 136–157. [CrossRef]

4. Chen, S.; Zhang, Z.; Jiang, W.; Zhang, S.; Zhu, J.; Wang, L.; Ou, H.; Zaman, S.; Tan, L.; Zhu, P.; et al. Engineering Water Molecules Activation Center on Multisite Electrocatalysts for Enhanced CO_2 Methanation. *Am. Chem. Soc.* **2022**, *144*, 12807–12815. [CrossRef] [PubMed]

5. Zaman, S.; Huang, L.; Douka, A.I.; Yang, H.; You, B.; Xia, B.Y. Oxygen Reduction Electrocatalysts toward Practical Fuel Cells: Progress and Perspectives. *Angew. Chem. Int. Ed.* **2021**, *60*, 17832–17852. [CrossRef]

6. Gao, C.; Zhang, X.; Zhan, J.; Cai, B. Engineering of aerogel-based electrocatalysts for oxygen evolution reaction. *Electrochem. Sci. Adv.* **2021**, *2*, e2100113. [CrossRef]

7. Li, L.; Wang, P.; Shao, Q.; Huang, X. Recent Progress in Advanced Electrocatalyst Design for Acidic Oxygen Evolution Reaction. *Adv. Mater.* **2021**, *33*, 2004243. [CrossRef]

8. Shan, J.; Ling, T.; Davey, K.; Zheng, Y.; Qiao, S.-Z. Transition-Metal-Doped RuIr Bifunctional Nanocrystals for Overall Water Splitting in Acidic Environments. *Adv. Mater.* **2019**, *31*, 1900510. [CrossRef]

9. Shan, J.; Guo, C.; Zhu, Y.; Chen, S.; Song, L.; Jaroniec, M.; Zheng, Y.; Qiao, S.-Z. Charge-Redistribution-Enhanced Nanocrystalline $Ru@IrO_x$ Electrocatalysts for Oxygen Evolution in Acidic Media. *Chem* **2019**, *5*, 445–459. [CrossRef]

10. Zaman, S.; Su, Y.-Q.; Dong, C.-L.; Qi, R.; Huang, L.; Qin, Y.; Huang, Y.-C.; Li, F.-M.; You, B.; Guo, W.; et al. Scalable Molten Salt Synthesis of Platinum Alloys Planted in Metal–Nitrogen–Graphene for Efficient Oxygen Reduction. *Angew. Chem. Int. Ed.* **2022**, *61*, e202115835. [CrossRef]

11. Zaman, S.; Tian, X.; Su, Y.-Q.; Cai, W.; Yan, Y.; Qi, R.; Douka, A.I.; Chen, S.; You, B.; Liu, H.; et al. Direct integration of ultralow-platinum alloy into nanocarbon architectures for efficient oxygen reduction in fuel cells. *Sci. Bull.* **2021**, *66*, 2207–2216. [CrossRef]

12. Cai, B.; Eychmüller, A. Promoting Electrocatalysis upon Aerogels. *Adv. Mater.* **2019**, *31*, 1804881. [CrossRef]

13. Stoerzinger, K.A.; Rao, R.R.; Wang, X.R.; Hong, W.T.; Rouleau, C.M.; Shao-Horn, Y. The Role of Ru Redox in pH-Dependent Oxygen Evolution on Rutile Ruthenium Dioxide Surfaces. *Chem* **2017**, *2*, 668–675. [CrossRef]

14. Reier, T.; Pawolek, Z.; Cherevko, S.; Bruns, M.; Jones, T.; Teschner, D.; Selve, S.; Bergmann, A.; Nong, H.N.; Schlögl, R.; et al. Molecular Insight in Structure and Activity of Highly Efficient, Low-Ir Ir–Ni Oxide Catalysts for Electrochemical Water Splitting (OER). *Am. Chem. Soc.* **2015**, *137*, 13031–13040. [CrossRef]

15. Wang, H.; Chen, Z.-n.; Wu, D.; Cao, M.; Sun, F.; Zhang, H.; You, H.; Zhuang, W.; Cao, R. Significantly Enhanced Overall Water Splitting Performance by Partial Oxidation of Ir through Au Modification in Core–Shell Alloy Structure. *J. Am. Chem. Soc.* **2021**, *143*, 4639–4645. [CrossRef]

16. Cao, L.; Luo, Q.; Chen, J.; Wang, L.; Lin, Y.; Wang, H.; Liu, X.; Shen, X.; Zhang, W.; Liu, W.; et al. Dynamic oxygen adsorption on single-atomic Ruthenium catalyst with high performance for acidic oxygen evolution reaction. *Nat. Commun.* **2019**, *10*, 4849. [CrossRef]

17. Lin, Y.; Tian, Z.; Zhang, L.; Ma, J.; Jiang, Z.; Deibert, B.J.; Ge, R.; Chen, L. Chromium-ruthenium oxide solid solution electrocatalyst for highly efficient oxygen evolution reaction in acidic media. *Nat. Commun.* **2019**, *10*, 162. [CrossRef]

18. Yao, Y.; Hu, S.; Chen, W.; Huang, Z.-Q.; Wei, W.; Yao, T.; Liu, R.; Zang, K.; Wang, X.; Wu, G.; et al. Engineering the electronic structure of single atom Ru sites via compressive strain boosts acidic water oxidation electrocatalysis. *Nat. Catal.* **2019**, *2*, 304–313. [CrossRef]

19. Batchelor, T.A.A.; Pedersen, J.K.; Winther, S.H.; Castelli, I.E.; Jacobsen, K.W.; Rossmeisl, J. High-Entropy Alloys as a Discovery Platform for Electrocatalysis. *Joule* **2019**, *3*, 834–845. [CrossRef]

20. George, E.P.; Raabe, D.; Ritchie, R.O. High-entropy alloys. *Nat. Rev. Mater.* **2019**, *4*, 515–534. [CrossRef]

21. Chen, P.-C.; Liu, X.; Hedrick James, L.; Xie, Z.; Wang, S.; Lin, Q.-Y.; Hersam Mark, C.; Dravid Vinayak, P.; Mirkin Chad, A. Polyelemental nanoparticle libraries. *Science* **2016**, *352*, 1565–1569. [CrossRef]

22. Miracle, D.B.; Senkov, O.N. A critical review of high entropy alloys and related concepts. *Acta Mater.* **2017**, *122*, 448–511. [CrossRef]

23. Huang, K.; Zhang, B.; Wu, J.; Zhang, T.; Peng, D.; Cao, X.; Zhang, Z.; Li, Z.; Huang, Y.J. Exploring the impact of atomic lattice deformation on oxygen evolution reactions based on a sub-5 nm pure face-centred cubic high-entropy alloy electrocatalyst. *J. Mater. Chem. A* **2020**, *8*, 11938–11947. [CrossRef]

24. Lei, Z.; Liu, X.; Wu, Y.; Wang, H.; Jiang, S.; Wang, S.; Hui, X.; Wu, Y.; Gault, B.; Kontis, P.; et al. Enhanced strength and ductility in a high-entropy alloy via ordered oxygen complexes. *Nature* **2018**, *563*, 546–550. [CrossRef] [PubMed]

25. Yeh, J.W.; Chen, S.K.; Lin, S.J.; Gan, J.Y.; Chin, T.S.; Shun, T.T.; Tsau, C.H.; Chang, S.Y. Nanostructured High-Entropy Alloys with Multiple Principal Elements: Novel Alloy Design Concepts and Outcomes. *Adv. Eng. Mater.* **2004**, *6*, 299–303. [CrossRef]

26. Guo, C.; Jiao, Y.; Zheng, Y.; Luo, J.; Davey, K.; Qiao, S.-Z. Intermediate Modulation on Noble Metal Hybridized to 2D Metal-Organic Framework for Accelerated Water Electrocatalysis. *Chem* **2019**, *5*, 2429–2441. [CrossRef]

27. Jin, Z.; Lv, J.; Jia, H.; Liu, W.; Li, H.; Chen, Z.; Lin, X.; Xie, G.; Liu, X.; Sun, S.; et al. Nanoporous Al-Ni-Co-Ir-Mo High-Entropy Alloy for Record-High Water Splitting Activity in Acidic Environments. *Small* **2019**, *15*, 1904180. [CrossRef] [PubMed]

28. Mesa, C.A.; Francàs, L.; Yang, K.R.; Garrido-Barros, P.; Pastor, E.; Ma, Y.; Kafizas, A.; Rosser, T.E.; Mayer, M.T.; Reisner, E.; et al. Multihole water oxidation catalysis on haematite photoanodes revealed by operando spectroelectrochemistry and DFT. *Nat. Chem.* **2020**, *12*, 82–89. [CrossRef]

29. Francàs, L.; Corby, S.; Selim, S.; Lee, D.; Mesa, C.A.; Godin, R.; Pastor, E.; Stephens, I.E.L.; Choi, K.-S.; Durrant, J.R. Spectroelectrochemical study of water oxidation on nickel and iron oxyhydroxide electrocatalysts. *Nat. Commun.* **2019**, *10*, 5208. [CrossRef]

30. Nong, H.N.; Falling, L.J.; Bergmann, A.; Klingenhof, M.; Tran, H.P.; Spöri, C.; Mom, R.; Timoshenko, J.; Zichittella, G.; Knop-Gericke, A.; et al. Key role of chemistry versus bias in electrocatalytic oxygen evolution. *Nature* **2020**, *587*, 408–413. [CrossRef]

31. Xie, M.; Xiong, X.; Yang, L.; Shi, X.; Asiri, A.M.; Sun, X. An $Fe(TCNQ)_2$ nanowire array on Fe foil: An efficient non-noble-metal catalyst for the oxygen evolution reaction in alkaline media. *Chem. Commun.* **2018**, *54*, 2300–2303. [CrossRef]

32. Zhu, W.; Zhu, G.; Yao, C.; Chen, H.; Hu, J.; Zhu, Y.; Liang, W. Porous amorphous FeCo alloys as pre-catalysts for promoting the oxygen evolution reaction. *J. Alloys Compd.* **2020**, *828*, 154465. [CrossRef]

33. Stern, L.-A.; Feng, L.; Song, F.; Hu, X. Ni_2P as a Janus catalyst for water splitting: The oxygen evolution activity of Ni_2P nanoparticles. *Energy Environ. Sci.* **2015**, *8*, 2347–2351. [CrossRef]

34. Bates, M.K.; Jia, Q.; Doan, H.; Liang, W.; Mukerjee, S. Charge-Transfer Effects in Ni–Fe and Ni–Fe–Co Mixed-Metal Oxides for the Alkaline Oxygen Evolution Reaction. *ACS Catal.* **2016**, *6*, 155–161. [CrossRef]

35. Ishaque, M.; Shah, A.; Iftikhar, F.J.; Akbar, M. Development of transition metal based electrolyzer for efficient oxygen evolution reaction. *J. Renew. Sustain. Energy* **2020**, *12*, 024102. [CrossRef]

36. Li, K.; Li, Y.; Peng, W.; Zhang, G.; Zhang, F.; Fan, X. Bimetallic Iron–Cobalt Catalysts and Their Applications in Energy-Related Electrochemical Reactions. *Catalysts* **2019**, *9*, 762. [CrossRef]

37. Saha, S.; Ganguli, A.K. FeCoNi Alloy as Noble Metal-Free Electrocatalyst for Oxygen Evolution Reaction (OER). *Chem.* **2017**, *2*, 1630–1636. [CrossRef]

38. Peng, Z.; Jia, D.; Al-Enizi, A.M.; Elzatahry, A.A.; Zheng, G. Electrocatalysts: From Water Oxidation to Reduction: Homologous Ni–Co Based Nanowires as Complementary Water Splitting Electrocatalysts. *Adv. Energy Mater.* **2015**, *5*, 1402031. [CrossRef]

39. Zou, X.; Goswami, A.; Asefa, T. Efficient Noble Metal-Free (Electro)Catalysis of Water and Alcohol Oxidations by Zinc–Cobalt Layered Double Hydroxide. *J. Am. Chem. Soc.* **2013**, *135*, 17242–17245. [CrossRef]

40. Dai, W.; Lu, T.; Pan, Y.J. Novel and promising electrocatalyst for oxygen evolution reaction based on MnFeCoNi high entropy alloy. *J. Power Sources* **2019**, *430*, 104–111. [CrossRef]

41. Li, D.; Wang, C.; Tripkovic, D.; Sun, S.; Markovic, N.M.; Stamenkovic, V.R. Surfactant Removal for Colloidal Nanoparticles from Solution Synthesis: The Effect on Catalytic Performance. *ACS Catal.* **2012**, *2*, 1358–1362. [CrossRef]

42. Jiang, K.; Luo, M.; Peng, M.; Yu, Y.; Lu, Y.-R.; Chan, T.-S.; Liu, P.; de Groot, F.M.F.; Tan, Y. Dynamic active-site generation of atomic iridium stabilized on nanoporous metal phosphides for water oxidation. *Nat. Commun.* **2020**, *11*, 2701. [CrossRef]

43. Zhang, J.; Liu, J.; Xi, L.; Yu, Y.; Chen, N.; Sun, S.; Wang, W.; Lange, K.M.; Zhang, B. Single-Atom Au/NiFe Layered Double Hydroxide Electrocatalyst: Probing the Origin of Activity for Oxygen Evolution Reaction. *J. Am. Chem. Soc.* **2018**, *140*, 3876–3879. [CrossRef] [PubMed]